Example Problem CO2-8
CO_2 Injection into a Hybrid Heterogeneous Domain

Abstract: *Geophysical field measurements combined with geostatistical techniques can yield complex geological models that have fully heterogeneous distributions of petrophysical properties. Typically only a limited number of parameters are distributed across the domain in a fully heterogeneous manner, such as porosity and intrinsic permeability. Parameters that define the relationships between capillary pressure, phase saturation, and phase relative permeability (ksP functions), are generally determined from measurements on discrete core samples. The STOMP simulator input routines have been designed to handle homogeneous, zoned, heterogeneous, and hybrid heterogeneous distributions of petrophysical properties. This problem considers the injection of CO_2 into a saline formation whose petrophysical properties of porosity and intrinsic permeability are fully heterogeneous, relative permeability-saturation-capillary pressure (ksP) function parameters are zoned, and all other parameters homogeneous, the hybrid heterogeneous distribution.*

Problem Description

This problem addresses complexity in formation petrology and geologic structure. Complexity in the petrology is introduced via a heterogeneous and anisotropic specification of intrinsic permeability, heterogeneous specification of porosity, combined with a zoned specification of relative permeability-saturation-capillary pressure (k-s-P) characteristics. The k-s-P functions additionally include hysteresis in the drainage and imbibition paths, nonwetting fluid entrapment, and extensions to drying below the wetting-fluid residual saturation. CO_2 is injected near the base of a hypothetical s-shaped geologic deep saline formation via a vertical well, adding structural complexity to the problem. The s-shaped formation is discretized using a boundary-fitted structure domain, making the vertical well trajectory not aligned with the principally grid axes. A relatively small two-dimensional domain (60 x 16) is specified for this problem to keep the emphasis on complexity in petrology and geologic structure and to shorten execution time. Two mirror-image computational grids are provided with the problem set. The base problem uses the left-to-right s-

shaped domain, and a problem exercise uses the right-to-left s-shaped domain.

The left-to-right computational grid is shown in Figure 1. The overall dimensions of the domain are 11.9 m in length (x-direction), 1.0 m in width (y-direction), and 7.5 m in height (z-direction). There are two coordinate systems for this problem, the global coordinate system shown in Figure 1, and the computational coordinate system, which follows the contours of the boundary-fitted grid. The computational coordinate system will be noted with primes. The x' (x-prime) direction follows the s-shaped domain from lower-right to upper left in Figure 1. Fluxes reported in the output files for this problem are in reference to the computational coordinate system (i.e., the primed directions). Boundary conditions refer to the primed directions, but the well model specifications are in terms of the global coordinate system (i.e., the unprimed directions). The physical domain for this problem is not representative of typical field-scale domain for carbon sequestration, but is useful for investigating simulation complexity. The computation domain is specified via a grid file, named s_shape_lr.grd. This file contains a list of the x-direction locations of 61 x 17 vertices, followed by a list of the z-direction locations of 61 x 17 vertices. The y-direction grid spacing is defaulted to 1.0 m.

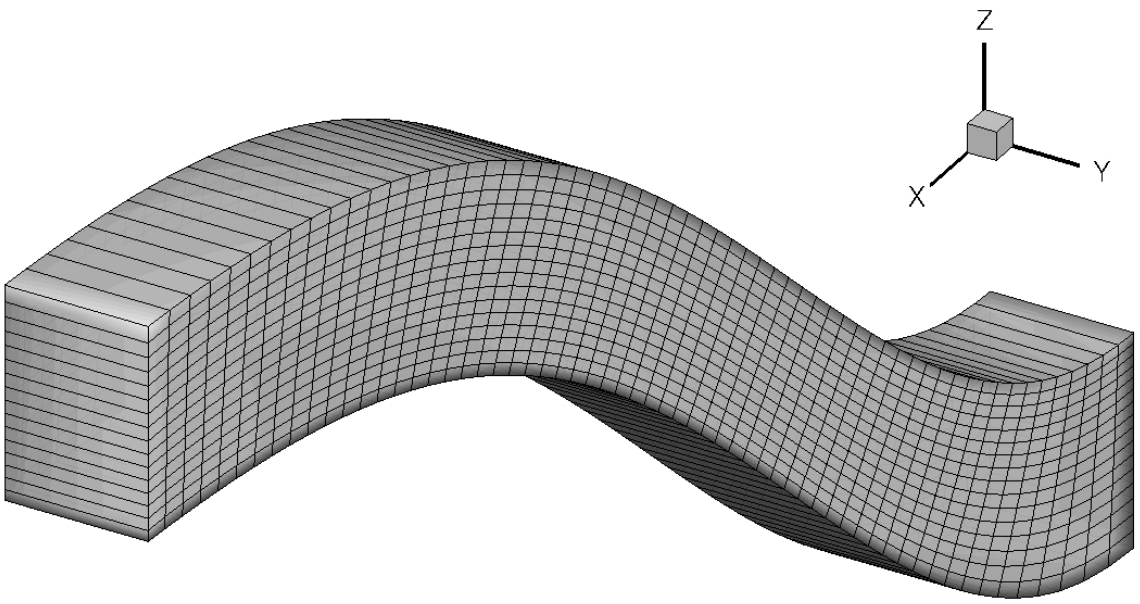

Figure 1. Schematic of the computational grid for the left-to-right domain

The domain porosity varies between roughly 0.15 and 0.22 across the domain as defined in the "porosity.dat" file, specified via the *Mechanical Properties Card*. A color-scaled image of the porosity distribution is shown in Figure 2. The intrinsic permeability is anisotropic, having different distributions in the x'- and z'-directions. The x'-direction intrinsic permeability varies between roughly 4 and 28 mD across the domain. A color-scaled image of the x'-direction intrinsic permeability is shown in Figure 3. The z'-direction intrinsic permeability varies between roughly 4 and 32 mD across the domain. A color-scaled image of the z'-direction intrinsic permeability is shown in Figure 4. Only two function and parameter sets are declared for each of the three k-s-P functions: 1) saturation relationship, 2) aqueous relative permeability relationship, and 3) gas permeability relationship. The k-s-P functions are distributed across the domain in a layered fashion, using the indexing file, "indexing.dat," which contains either a 1 or 2 for each grid cell in the computational domain. The layered distribution of k-s-P functions is shown in Figure 5, where the blue represents index #1 and the green #2.

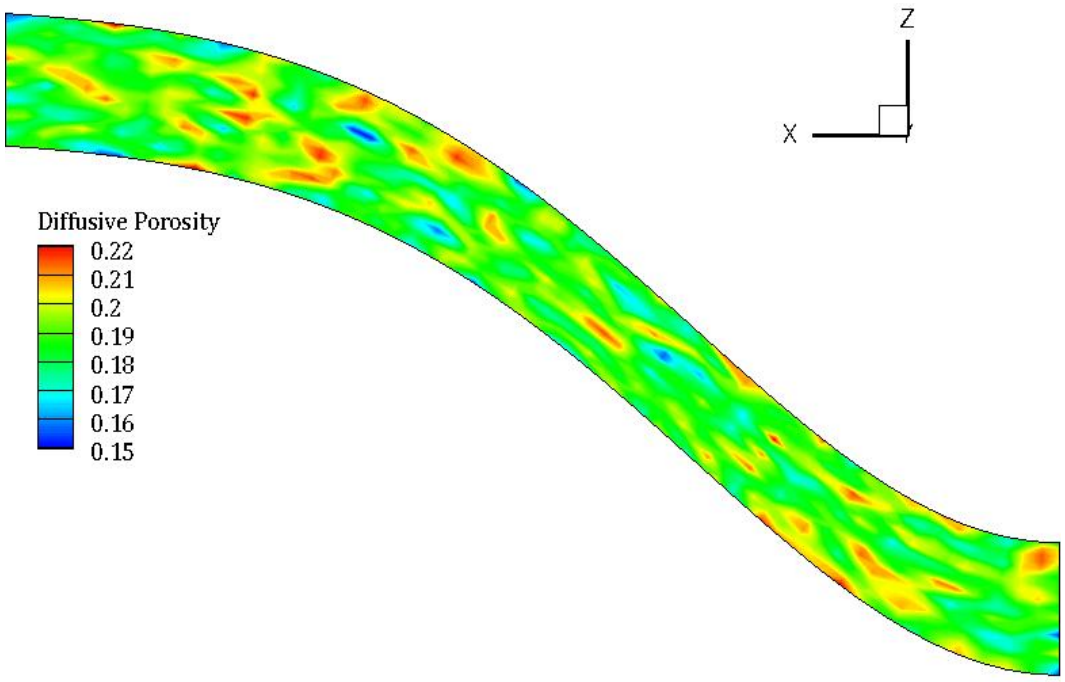

Figure 2. Porosity distribution specified via the "porosity.dat" file

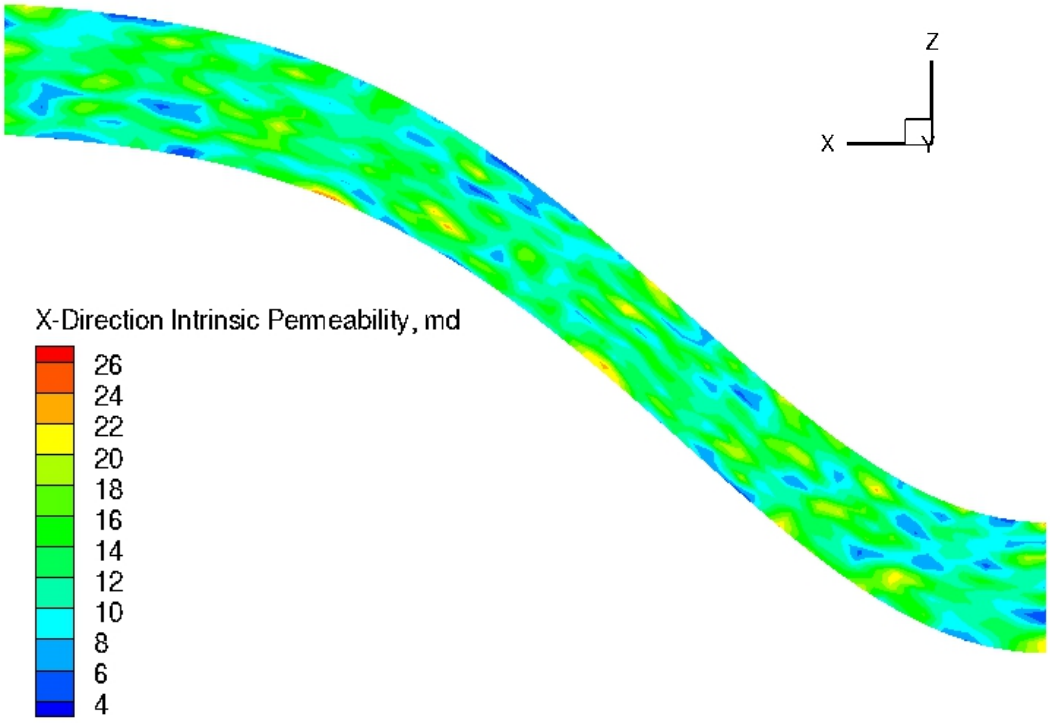

Figure 3. X′-direction intrinsic permeability distribution specified via the "permx.dat" file

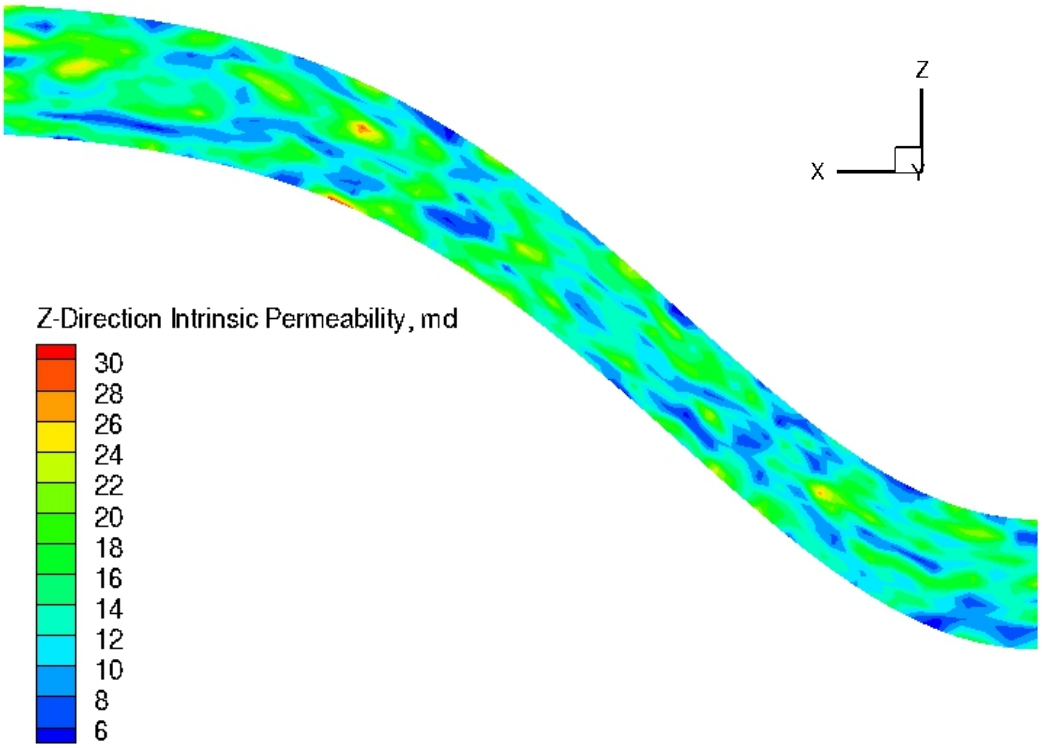

Figure 4. Z′-direction intrinsic permeability distribution specified via the "permz.dat" file.

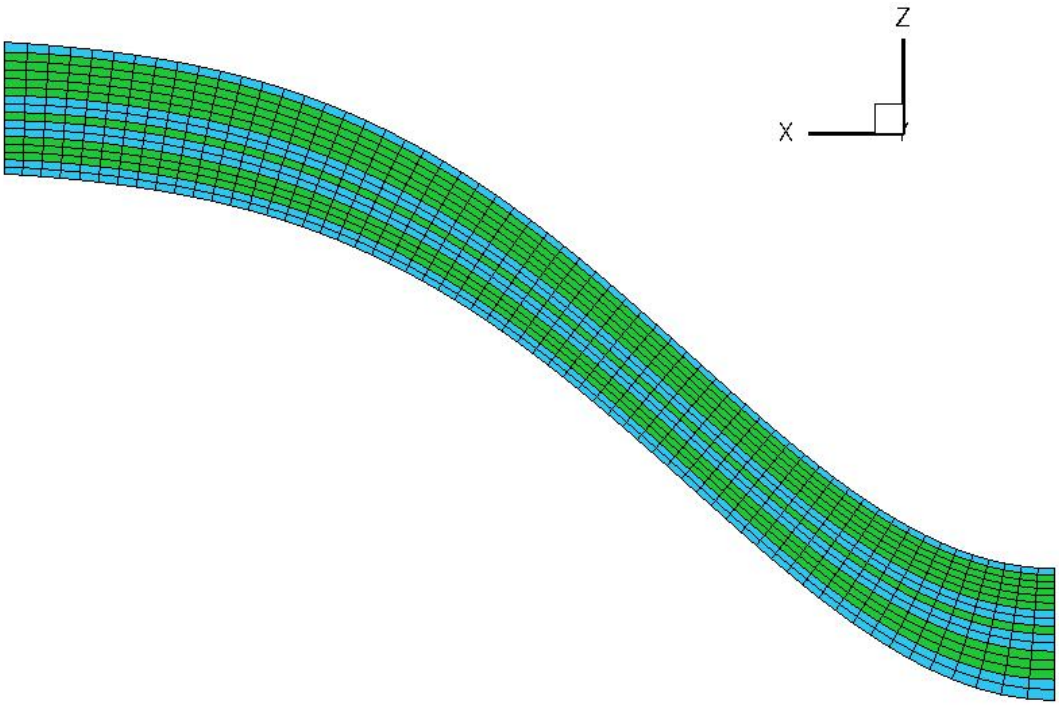

Figure 5. k-s-P function distribution specified via the "indexing.dat" file

For STOMP-CO2, the aqueous phase is the wetting phase and the CO^2 dominate phase (i.e., gas phase) is the non-wetting phase. The relationship between aqueous saturation and gas-aqueous capillary pressure was specified as being hysteretic and extending below the aqueous residual saturation. The core function was the Brooks and Corey function (1966) and the extension below aqueous saturation was that of Webb (2000). The Brooks and Corey (1966) correlation is a three-parameter function that makes use of an entry pressure to inhibit desaturation for scaled capillary pressures below the entry pressure:

$$\begin{aligned} &for\ \ \beta_{gl}\, h_{gl} \le \varphi :\ \ \bar{s}_l = \frac{s_l - s_{lr}}{1 - s_{lr}} = 1 \\ &for\ \ \beta_{gl}\, h_{gl} > \varphi :\ \ \bar{s}_l = \frac{s_l - s_{lr}}{1 - s_{lr}} = \left(\frac{\varphi}{\beta_{gl}\, h_{gl}} \right)^{\lambda} ;\ \ h_{gl} = \left(\frac{P_g - P_l}{\rho_l^*\, g} \right) \end{aligned} \tag{1}$$

The Webb (2000) extension divides the capillary pressure-saturation function into two regimes. For low aqueous saturation the function follows a logarithmic form, and for moderate to high saturations the function follows the specified form (e.g., Brooks and Corey). Transition between the two forms occurs at the matching point, which occurs at the point where the two functions have matching slopes. The low-saturation function is a linear function on a semilog plot:

$$s_l = \frac{\log\left(\frac{h_{gl}}{h_{gl}^{mp}}\right)}{\gamma} + s_l^{mp};\ \gamma = -\frac{\log\left(\frac{h_{od}}{h_{gl}^{mp}}\right)}{s_l^{mp}} \tag{2}$$

The matching point saturation and capillary pressure head is determined by setting the partial derivative of the aqueous saturation with respect to the capillary pressure head in Eqn. (2) equal to the partial derivative of the aqueous saturation with respect to the capillary pressure head in the Brooks and Corey function, Eqn. (1), setting the capillary pressure head to the matching point capillary pressure head, setting the aqueous saturation to the matching point aqueous saturation and solving for the matching point aqueous saturation. A nonlinear solve is required to determine the matching point saturation and capillary pressure head for the Brooks and Corey, Eqn. (1), function, but this solution is only required once, during simulation initialization. An oven-dried head of 10^9 Pa (~10^5 m) is used for the Webb extension model.

Gas entrapment is assumed to occur only when the aqueous phase is on an imbibition path (i.e., increasing aqueous saturation). Gas saturation can be free or trapped:

$$s_g = 1 - s_l = s_{gf} + s_{gt} \tag{3}$$

where the trapped gas is assumed to be in the form of aqueous occluded ganglia and immobile. A complete theoretical model for scanning path hysteresis and nonwetting fluid entrapment was developed by Parker and Lenhard (1987). The entrapment model used in the STOMP-CO2 and -CO2e simulators is formulated after the simplifications of the Parker and Lenhard model published by Kaluarachchi and Parker (1992). The

potential effective trapped gas saturation varies between zero and the effective maximum trapped gas saturation as a function of the historical minimum value of the apparent aqueous saturation:

$$\begin{aligned}
&\bar{s}_{gt}^{potential} = \frac{s_{gt}^{potential}}{1-s_{lr}} = \bar{s}_{gt}^{\max}\left(\frac{1-\bar{\bar{s}}_l^{\min}}{1-\bar{\bar{s}}_l^{\min}\left(1+\bar{s}_{gt}^{\max}\right)}\right) = \left(\frac{1-\bar{\bar{s}}_l^{\min}}{1-R\left(1-\bar{\bar{s}}_l^{\min}\right)}\right) \\
&\bar{\bar{s}}_l^{\min} = \bar{s}_l^{\min} = \frac{s_l^{\min}-s_{lr}}{1-s_{lr}};\ R = \frac{1}{\bar{s}_{gt}^{\max}} - 1 \\
&\bar{\bar{s}}_l = \bar{s}_l + \bar{s}_{gt} = \frac{s_l + s_{gt} - s_{lr}}{1-s_{lr}};\ \bar{s}_l = \frac{s_l - s_{lr}}{1-s_{lr}};\ \bar{s}_{gt} = \frac{s_{gt}}{1-s_{lr}}
\end{aligned} \tag{4}$$

where *R* is the Land's parameter (1968). The effective trapped gas saturation varies between zero and the effective potential trapped gas saturation as a function of the apparent aqueous saturation:

$$\bar{s}_{gt} = \frac{s_{gt}}{1-s_{lr}} = \left(\frac{1-\bar{\bar{s}}_l^{\min}}{1-R\left(1-\bar{\bar{s}}_l^{\min}\right)}\right) - \left(\frac{1-\bar{\bar{s}}_l}{1-R\left(1-\bar{\bar{s}}_l\right)}\right) \tag{5}$$

The modeling of gas entrapment is optional in STOMP-CO2 and -CO2e. When the gas entrapment model is active, the effective aqueous saturation in Eqn. (1) is replaced with the apparent aqueous saturations, which makes the apparent aqueous saturations a function of the capillary pressure.

The entrapment of a nonwetting fluid by the imbibition of a wetting fluid yields differences in the relationship between capillary pressure and actual saturations depending whether the geologic media is on a drainage or imbibition path relative to the wetting fluid. Factors other than nonwetting fluid entrapment can yield hysteresis between the drainage and imbibition paths (i.e., relationships between the capillary pressure and saturation). The drainage-imbibition option in allows the user to specify unique functions for drainage and imbibition paths. The transition between drainage

and imbibition paths is dependent on a single historical reversal point (expressed as the minimum effective aqueous saturation) from drainage to imbibition. At the start of a simulation the historical reversal point is the effective aqueous saturation. During the simulation the historical reversal point is the minimum of the minimum effective aqueous saturation and the apparent aqueous saturation. The apparent aqueous saturation will be greater than the minimum effective aqueous saturation whenever there has been a reversal from drainage to imbibition. Reversals from imbibition to drainage follow the same transition path from drainage to imbibition, returning to the minimum effective aqueous saturation. During the transition between drainage and imbibition paths and intermediate scanning path is followed:

$$\bar{\bar{s}}_l = \left[\frac{\bar{\bar{s}}_l^{\min}}{\bar{\bar{s}}_l} \right] \bar{\bar{s}}_l^d \left(h \right) + \left[1 - \frac{\bar{\bar{s}}_l^{\min}}{\bar{\bar{s}}_l} \right] \bar{\bar{s}}_l^i \left(h \right) \tag{6}$$

Solving for the apparent aqueous saturation yields a quadratic form, which can be solved directly depending on the values for the apparent aqueous saturation from the drainage and imbibition functions:

$$\begin{aligned} &\textit{if} \quad \bar{\bar{s}}_l^d \left(h \right) \geq \bar{\bar{s}}_l^i \left(h \right) \\ &\bar{\bar{s}}_l = \frac{\bar{\bar{s}}_l^i \left(h \right) + \sqrt{\left(\bar{\bar{s}}_l^i \left(h \right) \right)^2 + 4\, \bar{\bar{s}}_l^{\min}\, \bar{\bar{s}}_l^d \left(h \right) - 4\, \bar{\bar{s}}_l^{\min}\, \bar{\bar{s}}_l^i \left(h \right)}}{2} \\ &\textit{else} \\ &\bar{\bar{s}}_l = \frac{\bar{\bar{s}}_l^i \left(h \right) - \sqrt{\left(\bar{\bar{s}}_l^i \left(h \right) \right)^2 + 4\, \bar{\bar{s}}_l^{\min}\, \bar{\bar{s}}_l^d \left(h \right) - 4\, \bar{\bar{s}}_l^{\min}\, \bar{\bar{s}}_l^i \left(h \right)}}{2} \end{aligned} \tag{7}$$

The hysteretic drainage and imbibition path option can be combined with the gas entrapment and extension below aqueous residual saturation options. The parameters for the aqueous saturation versus capillary pressure functions described in Eqns. (1) through (7) are listed in Table 1, for the two *Rock/Soil Zonation* indices. Also listed in Table 1 are the matching point saturations and capillary heads, computed internally.

Table 1. Brooks and Corey drainage and imbibition function parameters

Property	Rock/Soil #1	Rock/Soil #2
Drainage Entry Head	$\psi^d = 0.33\ m$	$\psi^d = 4.14\ m$
Drainage Exponent	$\lambda^d = 1.44$	$\lambda^d = 1.816$
Aqueous Residual Sat.	$s_{lr} = 0.3$	$s_{lr} = 0.4$
Imbibition Entry Head	$\psi^i = 0.11\ m$	$\psi^i = 1.45\ m$
Imbibition Exponent	$\lambda^i = 1.44$	$\lambda^i = 2.32$
Actual Gas Residual Sat.	$s_{gr} = 0.107$	$s_{gr} = 0.188$
Drainage Matching Point Saturation	$s^d_{mp} = 0.3218$	$s^d_{mp} = 0.4280$
Drainage Matching Point Head	$h^d_{mp} = 3.667\ m$	$h^d_{mp} = 22.40\ m$
Imbibition Matching Point Saturation	$s^i_{mp} = 0.3197$	$s^i_{mp} = 0.4187$
Imbibition Matching Point Head	$h^i_{mp} = 1.312\ m$	$h^i_{mp} = 6.471\ m$

Aqueous relative permeability was modeled using a modified Corey (1977):

$$k_{rl} = a\left(\bar{s}_l\right)^b$$
$$k_{rl} = a\left(\frac{s_l - s_{lr}}{1 - s_{lr} - s_{gr}}\right)^b \tag{8}$$

Hysteresis in the aqueous relative permeability was not considered. The parameters for the aqueous relative permeability versus aqueous saturation function described in Eqn. (8) are listed in Table 2, for the two *Rock/Soil Zonation* indices.

Table 2. Aqueous relative permeability function parameters

Property	Rock/Soil #1	Rock/Soil #2
End Point Relative Permeability	$a = 1.0$	$a = 1.0$
Exponent	$b = 2.0$	$b = 4.0$
Aqueous Residual Sat.	$s_{lr} = 0.3$	$s_{lr} = 0.4$
Gas Residual Sat.	$s_{gr} = 0.031$	$s_{gr} = 0.005$

The gas relative permeability was modeled using a hysteretic form Doughty (2009) function, which is a two-exponent function. The Doughty function has been extended to include separate curves for drainage and imbibition paths; where the apparent aqueous saturation for the drainage and imbibition paths are defined using the trapped gas and maximum trapped gas saturations, respectively.

$$k_{rg}^{d} = k_{rg}^{\max}\left[1-\bar{\bar{s}}_l^{d}\right]^{\gamma}\left[1-\left(\bar{\bar{s}}_l^{d}\right)^{1/m}\right]^{2m};\; k_{rg}^{i} = k_{rg}^{max}\left[1-\bar{\bar{s}}_l^{i}\right]^{\gamma}\left[1-\left(\bar{\bar{s}}_l^{i}\right)^{1/m}\right]^{2m}$$
$$\bar{\bar{s}}_l^{i} = \bar{s}_l + \bar{s}_{gt}^{\max} = \frac{s_l + s_{gt}^{\max} - s_{lr}^{i}}{1-s_{lr}^{i}};\; \bar{\bar{s}}_l^{d} = \bar{s}_l + \bar{s}_{gt} = \frac{s_l + s_{gt} - s_{lr}^{d}}{1-s_{lr}^{d}} \tag{9}$$

The gas relative permeability for any scanning path is determined using scaling between the drainage and imbibition paths with the historical minimum apparent aqueous saturation and the apparent aqueous saturation

$$k_{rg} = \left[\frac{\bar{\bar{s}}_l^{\min}}{\bar{\bar{s}}_l}\right]k_{rg}^{d} + \left[1-\frac{\bar{\bar{s}}_l^{\min}}{\bar{\bar{s}}_l}\right]k_{rg}^{i} \tag{10}$$

The parameters for the gas relative permeability versus aqueous saturation function described in Eqns. (9) and (10) are listed in Table 3, for the two *Rock/Soil Zonation*

indices.

Table 3. Gas relative permeability function parameters.

Property	Rock/Soil #1	Rock/Soil #2
End Point Relative Permeability	$k_{rg}^{\max} = 1.5$	$k_{rg}^{\max} = 0.92$
γ Exponent	$\gamma = 0.4$	$\gamma = 1.05$
Drainage Aqueous Residual Saturation	$s_{lr}^{d} = 0.53$	$s_{lr}^{d} = 0.771$
m Exponent	$m = 0.9$	$m = 0.92$
Imbibition Aqueous Residual Saturation	$s_{lr}^{i} = 0.62$	$s_{lr}^{i} = 0.79$
Imbibition Max. Trapped Gas Saturation	$s_{gt}^{\max} = 0.115$	$s_{gt}^{\max} = 0.013$

Specifying initial conditions and boundary conditions for boundary-fitted grids can quickly become burdensome if done manually. This problem using STOMP-CO2 features that simplify the process: 1) hydrostatic initial conditions and 2) initial condition boundary conditions. The hydrostatic initial condition option allows the user to specify a system pressure at a global z-direction elevation, a temperature at a global z-direction elevation, a z-direction temperature gradient (i.e., geothermal gradient), an aqueous salt mass fraction at a global z-direction elevation, and a aqueous salt mass fraction gradient in the z-direction. STOMP-CO2 then uses this information to compute the initial conditions across the computational domain. The z-direction elevations specified with this option must be with respect to the global coordinate system used to defined the computational grid, but the z-direction elevations need not be within the computational domain, although that is preferred. The data for the hydrostatic initial condition specification are listed in Table 4. The initial condition boundary condition option, specifies that the grid cell initial conditions will be applied to boundary surfaces. Temperature and aqueous salt mass fractions are applied directly to the boundary surface. Fluid pressures are adjusted using hydrostatic equilibrium from the grid-cell centroid to the boundary surface centroid. Pressure adjustments may alter the dissolved CO_2 concentrations, fluid properties, and fluid saturations on the boundary surface. Once set the initial condition boundary surfaces are treated as Dirichlet type

boundaries, allowing fluid flow and heat transport across the boundary surface.

Table 4. Hydrostatic initial condition parameters.

Property	Value
Pressure	30.81955 MPa
Z-Direction Elevation	0.0 m
Temperature	100.0 ˚C
Z-Direction Elevation	0.0 m
Geothermal Gradient	-0.03 ˚C/m
Aqueous Salt Mass Fraction	0.1
Z-Direction Elevation	0.0 m
Salt Mass Fraction Gradient	0.0 1/m

Simulation Results

The problem simulation involves the injection of 2 kg/hr of dry CO_2 for a period of 4 days into the s-shaped formation with a maximum pressure at the top of the screened interval of 45 MPa. After the 4-day injection period CO_2 migrates under buoyancy forces and becomes entrapped. The integrated amounts of total CO_2, aqueous CO_2, gas CO_2, and trapped-gas CO_2 mass were requested in the *Output Control Card* under the reference node section. These integrated amounts are plotted versus time in Figure 6. The total CO_2 mass increases linearly during the 4-day injection period, indicating the well remains flow controlled. A slight loss in total CO_2 mass occurs as some of the CO_2 leaves the domain out the upper vertical boundary surface. Most of the CO_2 mass appears as an immiscible CO_2-rich phase (i.e., gas), but the percentage of this amount decreases over time as CO_2 dissolves into the aqueous phase. Trapped gas only occurs after the 4-day injection period, when the aqueous phase re-imbibes into the gas occupied pore space.

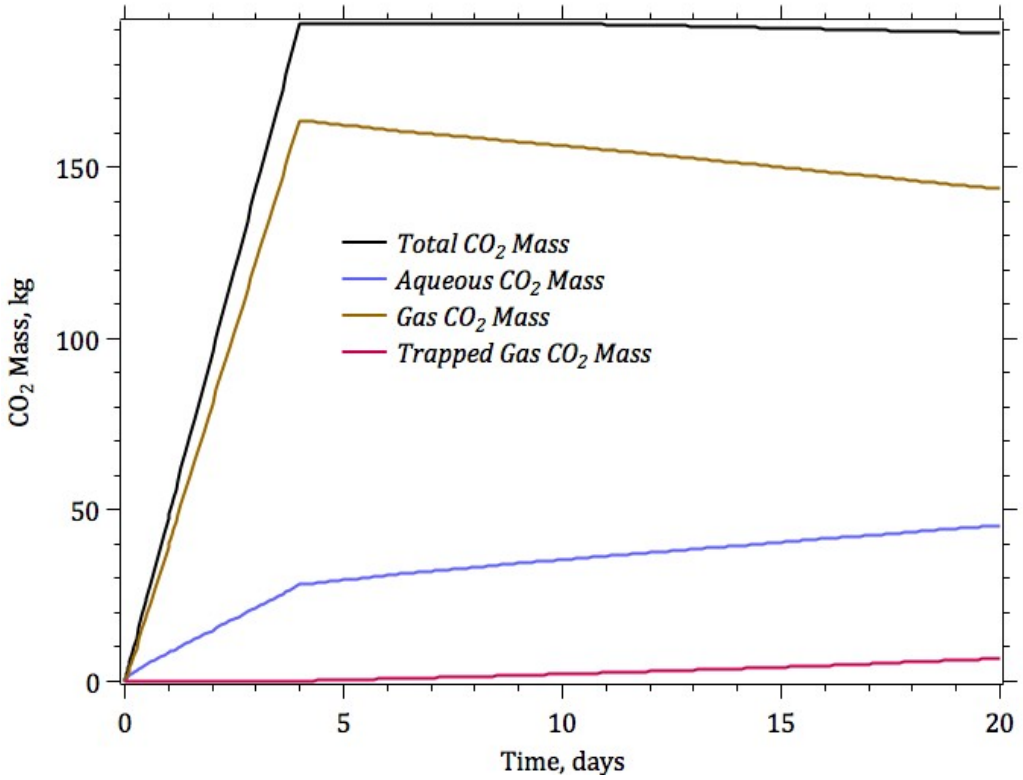

Figure 6. Total, aqueous, gas, and trapped gas integrated CO_2 mass versus time

A time series of color-contoured plots of gas saturation are shown in Figures 7a through 7f, at 0.1, 0.5, 1.0, 5.0, 10.0, and 20.0 days, respectively. CO_2 injected through the well, predominately enters into the layers where the gas relative permeability is higher. There is little indication of the heterogeneity in the intrinsic permeability in the gas saturation profiles. During and after the injection period the injected CO_2 migrates up the slope of the s-shaped basin. After the 4-day injection period the CO_2 migration rate slows, as the well pressure decays. Around 10 days the CO_2-rich phase (i.e., supercritical fluid) reaches the upper boundary surface, which is open to aqueous and gas flow. Trapped gas does not appear until around 10 days, Figures 8a and 8b. Aqueous phase imbibing into pore space occupied by gas phase, yielding trapped gas flows countercurrent to the buoyant gas phase. Trapped gas occurs at the receding end of the upward migrating gas plume.

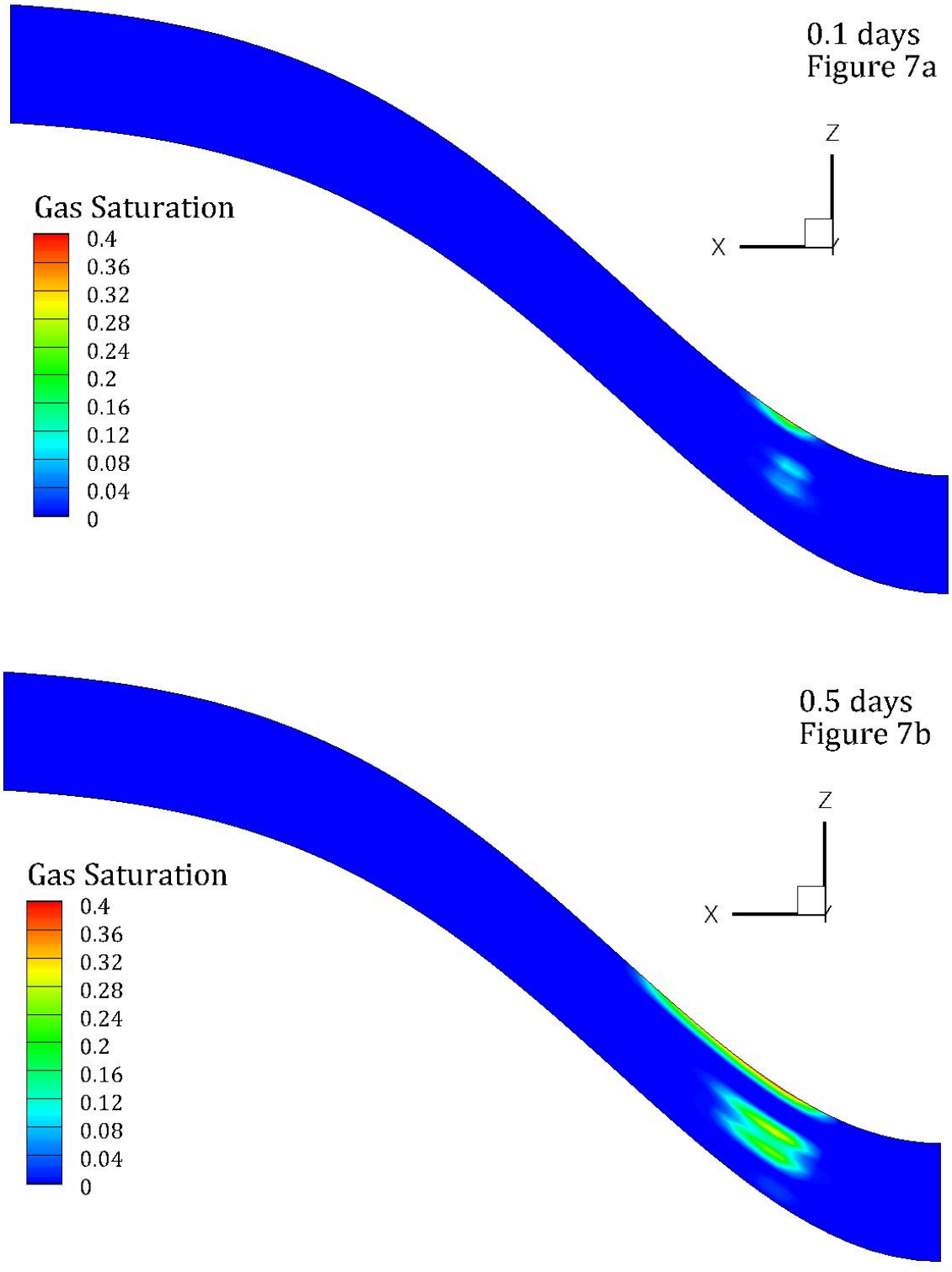

Figures 7a-b. Gas saturation at 0.1 and 0.5 days

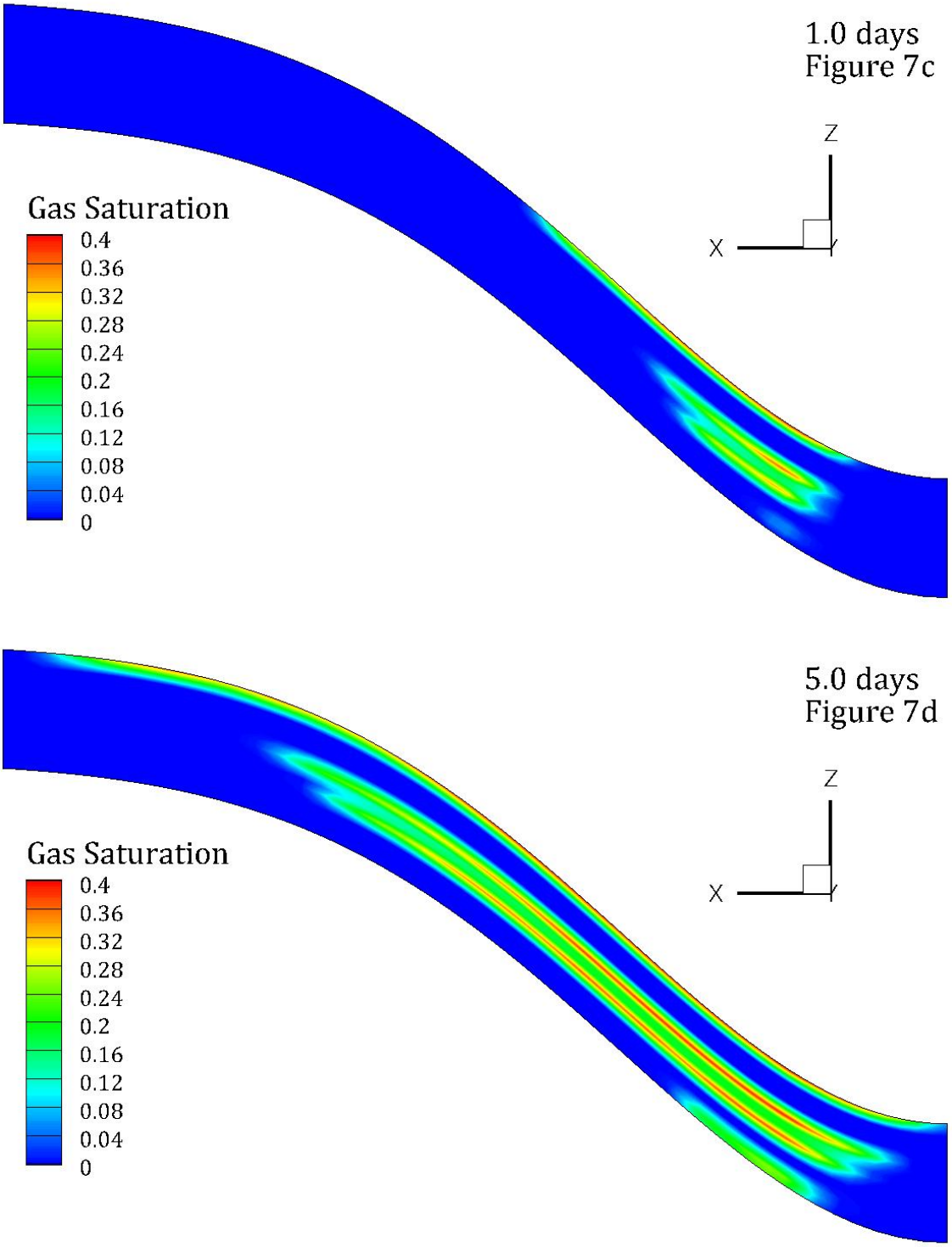

Figures 7c-d. Gas saturation at 1.0 and 5.0 days

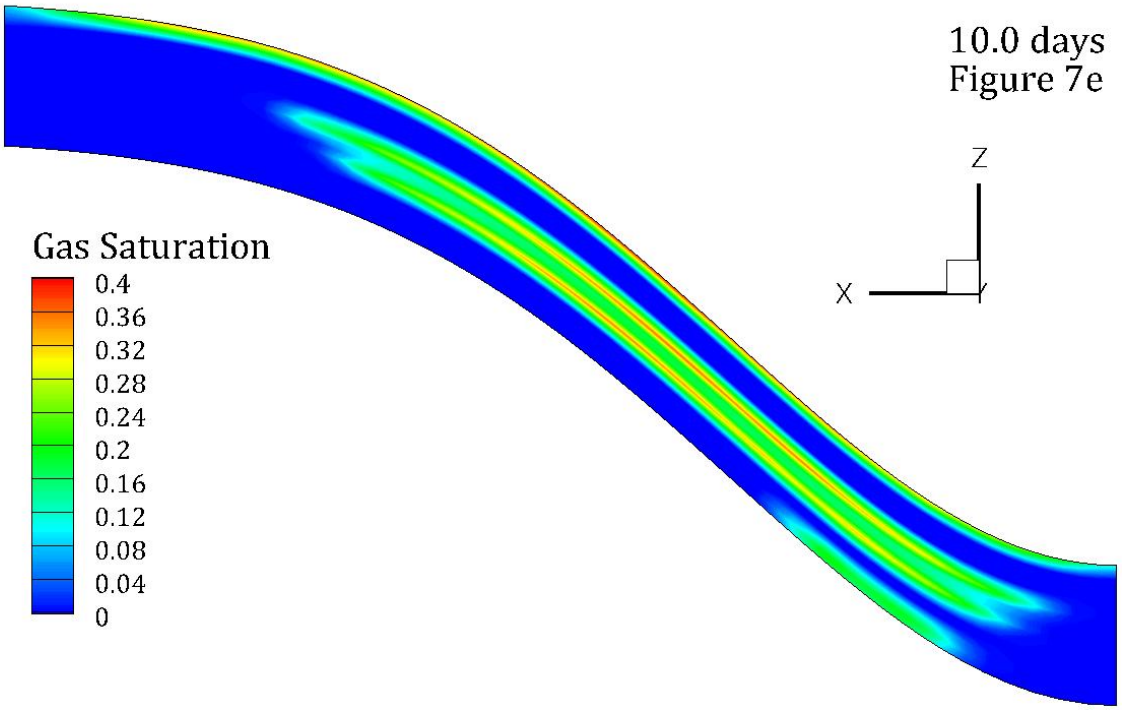

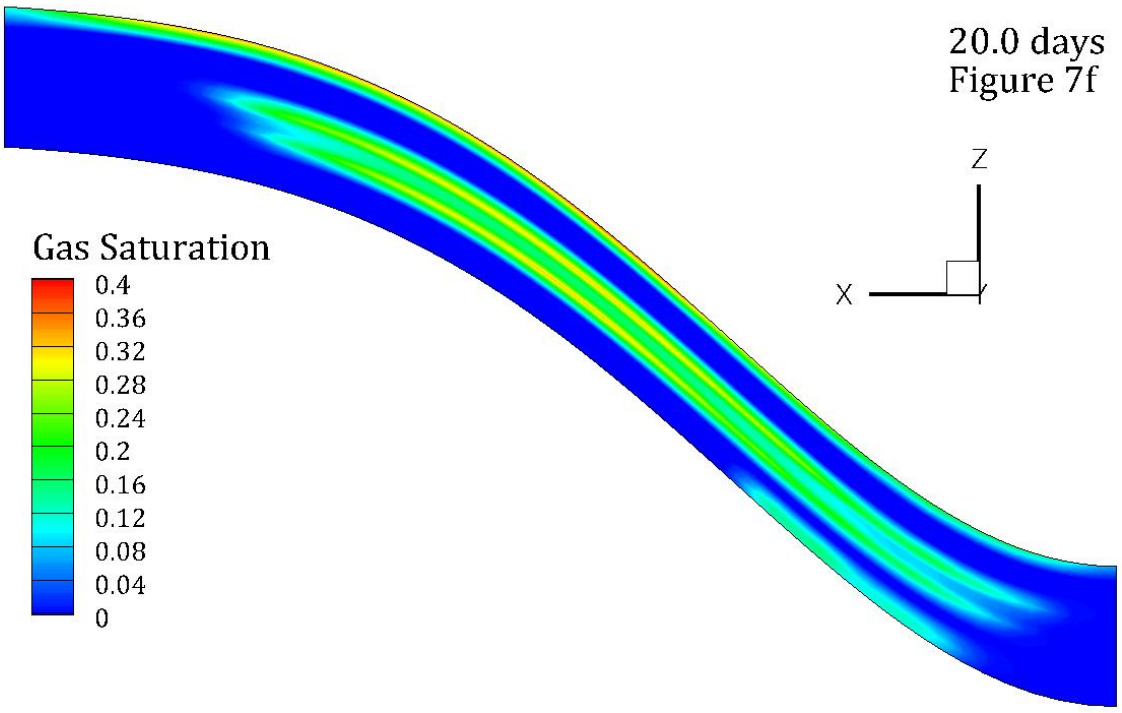

Figures 7e-f. Gas saturation at 10.0 and 20.0 days

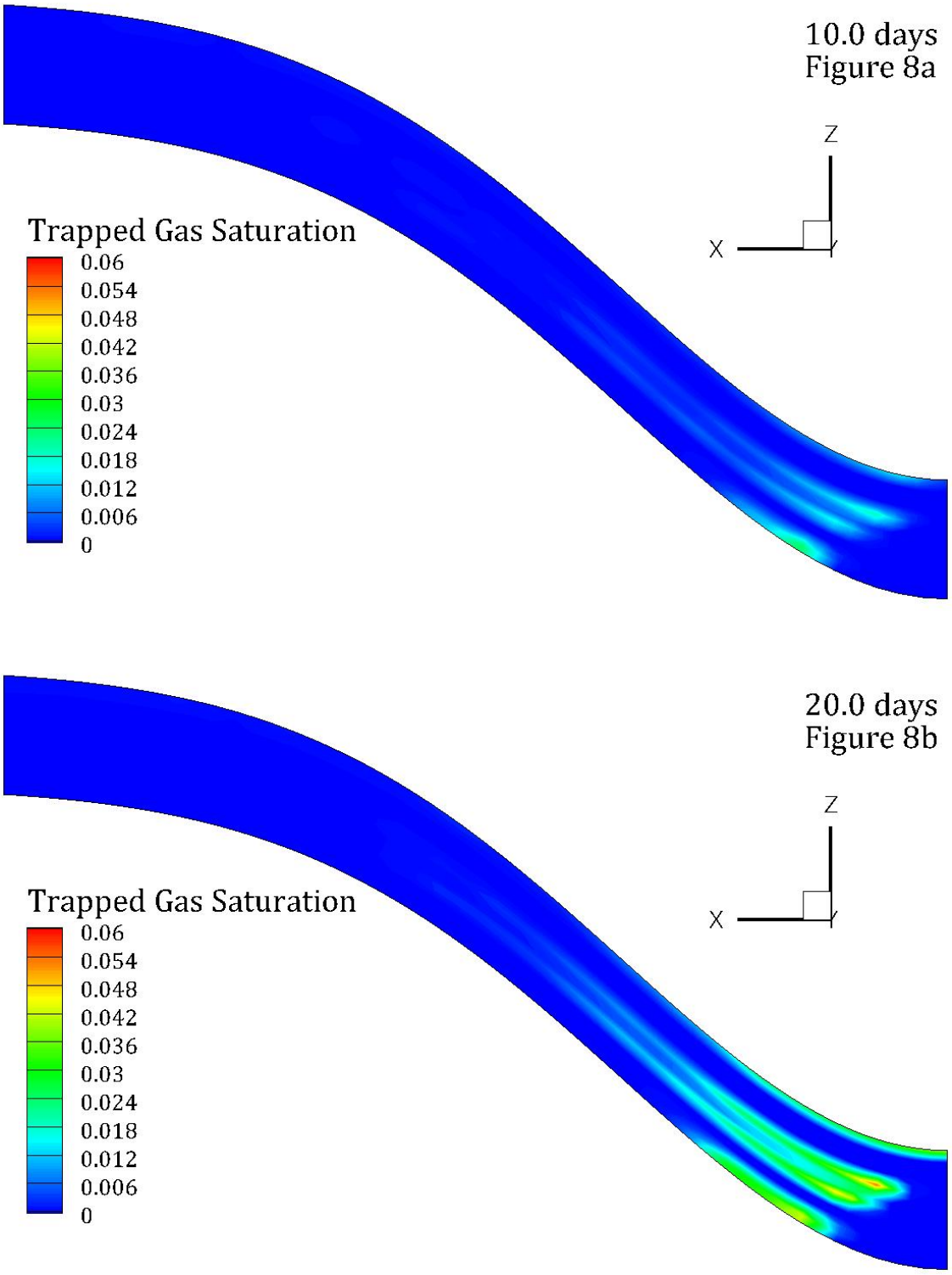

Figures 8a-b. Trapped gas saturation at 10.0 and 20.0 days

References

Brooks, R. H., and A. T. Corey. 1966. "Properties of porous media affecting fluid flow." *Journal of Irrigation and Drainage Division* 93(3):61-88.

Doughty, C. 2009. User's Guide for Hysteretic Capillary Pressure and Relative Permeability Functions in iTOUGH2, Lawrence Berkeley National Laboratory, LBNL-2483E.

Kaluarachchi, J.J. and J.C. Parker. 1992. "Multiphase flow with a simplified model for oil entrapment." Transport in Porous Media 7:1-14.

Land, C. S. 1968. "Calculation of imbibition relative permeability for two- and three-phase flow from rock properties." Trans. Am. Inst. Min. Metall. Pet. Eng. 243:149-156.

Parker, J. C. and R. J. Lenhard. 1987. "A model for hysteretic constitutive relations governing multiphase flow 1. Saturation-pressure relations." Water Resources Research, 23(12):2187- 2196.

Webb, S. W., 2000. "A simple extension of two-phase characteristic curves to include the dry region." *Water Resources Research*, 36(6):1425-1430.

Exercises

1. (Moderate) Check the Webb matching points reported in Table 1.
2. (Moderate) Use only the drainage scanning path for the saturation function, eliminate gas entrapment, and compare the CO_2-rich fluid (i.e., gas) plume history against the base simulation.
3. (Moderate) Move the injection well to the center of the s-shaped basin and compare the CO_2-rich fluid (i.e., gas) plume history against the base simulation.
4. (Difficult) Increase the range of heterogeneity in intrinsic permeability to see an impact of the CO_2-rich fluid plume migration pattern.

Input File

```
~Simulation Title Card
1,
STOMP Example Problem CO2-8,
Mark White,
Pacific Northwest Laboratory,
01 June 2011,
09:37 PDT,
1,
CO2 injection into a hybrid hetergeneous s-shaped domain.
```

```
~Solution Control Card
Normal,
STOMP-CO2,
1,
0,day,20,day,0.01,s,0.1,day,1.25,16,1.e-06,0.001,s,0.2,
1000,
Variable Aqueous Diffusion,
Variable Gas Diffusion,
0,

~Grid Card
Orthogonal,
60,1,16,
s_shape_lr.grd,m,

~Rock/Soil Zonation Card
IJK Indexing,

~Mechanical Properties Card
IJK Indexing,2650,kg/m^3,file:porosity.dat,file:porosity.dat,Pore Compressibility,3.0e-
6,1/psi,,,Millington and Quirk,

~Hydraulic Properties Card
IJK Indexing,file:permx.dat,mD,file:permy.dat,mD,file:permz.dat,mD,0.8,0.8,

~Saturation Function Card
IJK Indexing,Rock/Soil Zonation,2,file:indexing.dat,
#Layer 1
Brooks-Corey Drainage-Imbibition w/Webb,0.33,m,1.44,0.3,0.11,m,1.44,0.107,
#Layer 2
Brooks-Corey Drainage-Imbibition w/Webb,4.14,m,1.816,0.4,1.45,m,2.32,0.188,

~Aqueous Relative Permeability Card
IJK Indexing,Rock/Soil Zonation,2,file:indexing.dat,
#Layer 1
Free Corey,1.0,2.0,0.3,0.031,
#Layer 2
Free Corey,1.0,4.0,0.4,0.005,

~Gas Relative Permeability Card
IJK Indexing,Rock/Soil Zonation,2,file:indexing.dat,
#Layer 1
Doughty Drainage-Imbibition,1.5,0.4,0.53,0.9,0.62,0.115,
#Layer 2
Doughty Drainage-Imbibition,0.92,1.05,0.771,0.92,0.79,0.013,

~Salt Transport Card
IJK Indexing,0.0,m,0.0,m,

~Initial Conditions Card
Hydrostatic,30.81955,MPa,0.0,m,100.0,C,0.0,m,-0.03,C/m,0.10,0.0,m,0.0,1/m,

~Boundary Conditions Card
1,
East,Aqu. Initial Condition,Gas Initial Condition,Aqu. Mass Frac.,
60,60,1,1,1,16,1,
0,s,,,,,,0.1,,,,
```

```
~Coupled Well Card
1,
CO2 Injection Well,Water Relative Saturation,1.0,1.0,1.0,0.383184,MMT,
1,
2.0,m,0.5,m,10,m,2.0,m,0.5,m,0.0,m,0.1,m,0.0,screened,
2,
0.0,day,2.0,kg/hr,45,MPa,0.0,
4.0,day,2.0,kg/hr,45,MPa,0.0,

~Output Options Card
4,
1,1,1,
60,1,1,
1,1,16,
60,1,16,
1,1,day,m,6,6,6,
17,
Phase Condition,,
Gas Saturation,,
Trapped Gas Saturation,,
Integrated CO2 Mass,kg,
Integrated CO2 Aqueous Mass,kg,
Integrated CO2 Gas Mass,kg,
Integrated CO2 Trapped-Gas Mass,kg,
Salt Aqueous Mass Fraction,,
CO2 Aqueous Mass Fraction,,
Gas Density,kg/m^3,
Aqueous Density,kg/m^3,
Gas Pressure,MPa,
Aqueous Pressure,MPa,
Diffusive Porosity,,
Coupled-Well Press,1,MPa,
Coupled-Well CO2 Mass Rate,1,kg/s,
Coupled-Well CO2 Mass Integral,1,kg,
6,
0.1,day,
0.5,day,
1.0,day,
5.0,day,
10.0,day,
20.0,day,
13,
Rock/Soil Type,,
Diffusive Porosity,,
X-Intrinsic Permeability,mD,
Z-Intrinsic Permeability,mD,
Gas Saturation,,
Trapped Gas Saturation,,
CO2 Aqueous Concentration,gm/cm^3,
Salt Aqueous Mass Fraction,,
CO2 Aqueous Mass Fraction,,
Gas Pressure,MPa,
Aqueous Pressure,MPa,
Gas Density,kg/m^3,
Aqueous Density,kg/m^3,

~Surface Flux Card
6,
```

Aqueous CO2 Mass Flux,kg/s,kg,West,1,1,1,1,1,16,
Gas CO2 Mass Flux,kg/s,kg,West,1,1,1,1,1,16,
Total CO2 Mass Flux,kg/s,kg,West,1,1,1,1,1,16,
Aqueous CO2 Mass Flux,kg/s,kg,East,60,60,1,1,1,16,
Gas CO2 Mass Flux,kg/s,kg,East,60,60,1,1,1,16,
Total CO2 Mass Flux,kg/s,kg,East,60,60,1,1,1,16,

Solutions to Selected Exercises

Exercise 1

Webb matching points occur where the slope of the standard capillary head versus saturation function matches the slope of the Webb logarithmic form. The slope of the Brooks and Corey saturation versus capillary head is found by differentiating the Brooks and Corey function, Eqn. (1), with respect to capillary head

$$\frac{\partial s_l}{\partial h} = -\left(\frac{\psi}{h}\right)^{\lambda}\left(\frac{\lambda}{h}\right)\left(1 - s_{lr}\right) \tag{11}$$

where the scaling factor has been set to 1.0. The slope of the Webb extension saturation with respect to capillary head, Eqn. (2), is dependent on the matching point saturation, matching point head and oven-dry head.

$$\frac{\partial s_l}{\partial h} = \frac{-s_{mp}}{h_{mp}\ln\left(\frac{h_{od}}{h_{mp}}\right)};\ h_{od} = 1.021\ x\ 10^5 \tag{12}$$

The drainage and imbibition saturation versus capillary pressure functions for the two Rock/Soil indices are shown in Figure 9, along with the saturation and capillary head matching points for each curve. The matching points are correct when Eqns. 11 and 12 yield the same slope at the matching point. As the matching point saturation and head are variables in Eqn. 12, the solution requires a iterative nonlinear approach. The values can be validated without a nonlinear solve, which is the objective of this exercise.

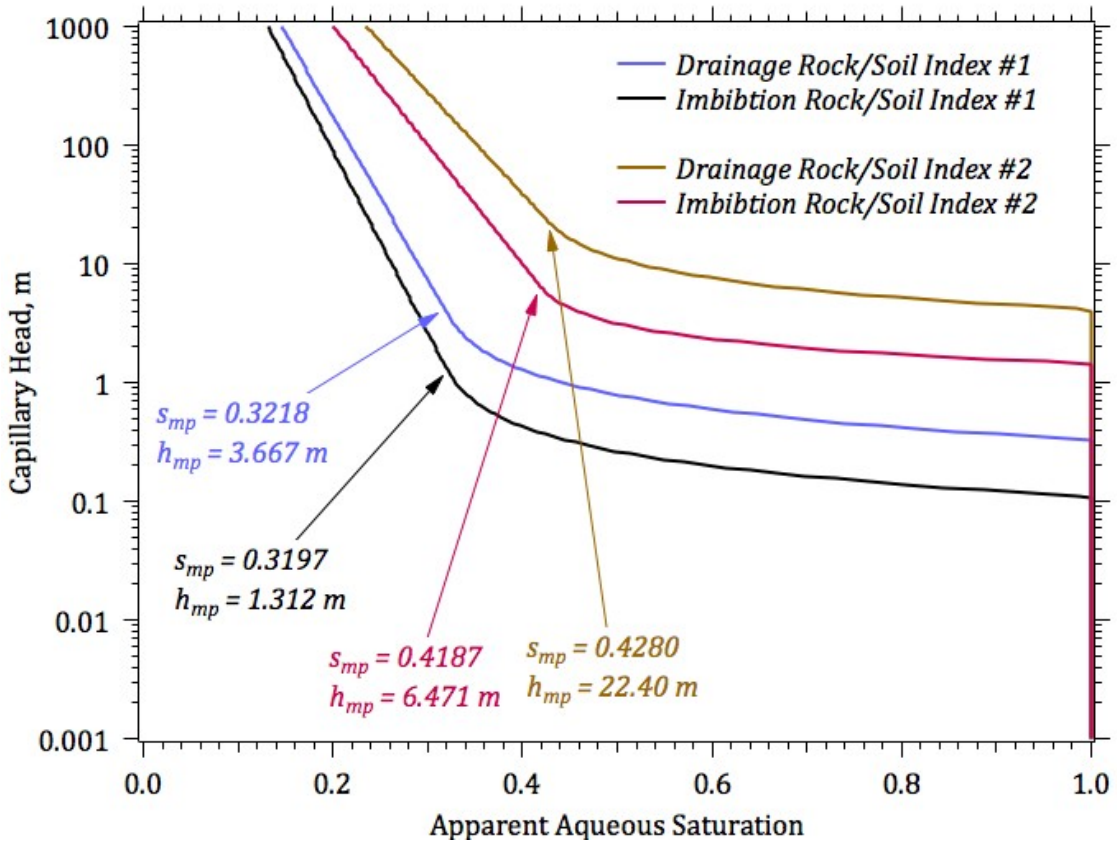

Figure 9. Drainage and imbibition capillary head versus saturation functions, showing Webb matching point saturations and capillary heads

Exercise 2

The *Drainage-Imbibition* option with the Brooks and Corey function specifies hysteresis between when the aqueous phase is draining and wetting. Without this option the Brooks and Corey function uses a single scanning path regardless of the wetting direction. A single drainage path can be specified by eliminating the *Drainage-Imbibition* option, using the drainage path parameters, and removing the imbibition path parameters. Without the *Entrapment* option the standard Brooks and Corey function does not include gas entrapment. All of the needed modifications to the input file are made in the *Saturation Function Card*, as shown below. Simulation results using only the drainage path parameters yield generally higher gas saturations, but the plume migration behavior is nearly identical, as shown in Figures 10a and 10b.

~Saturation Function Card
IJK Indexing,Rock/Soil Zonation,2,file:indexing.dat,
#Layer 1
Brooks-Corey w/Webb,0.33,m,1.44,0.3, ,
#Layer 2
Brooks-Corey w/Webb,4.14,m,1.816,0.4, ,

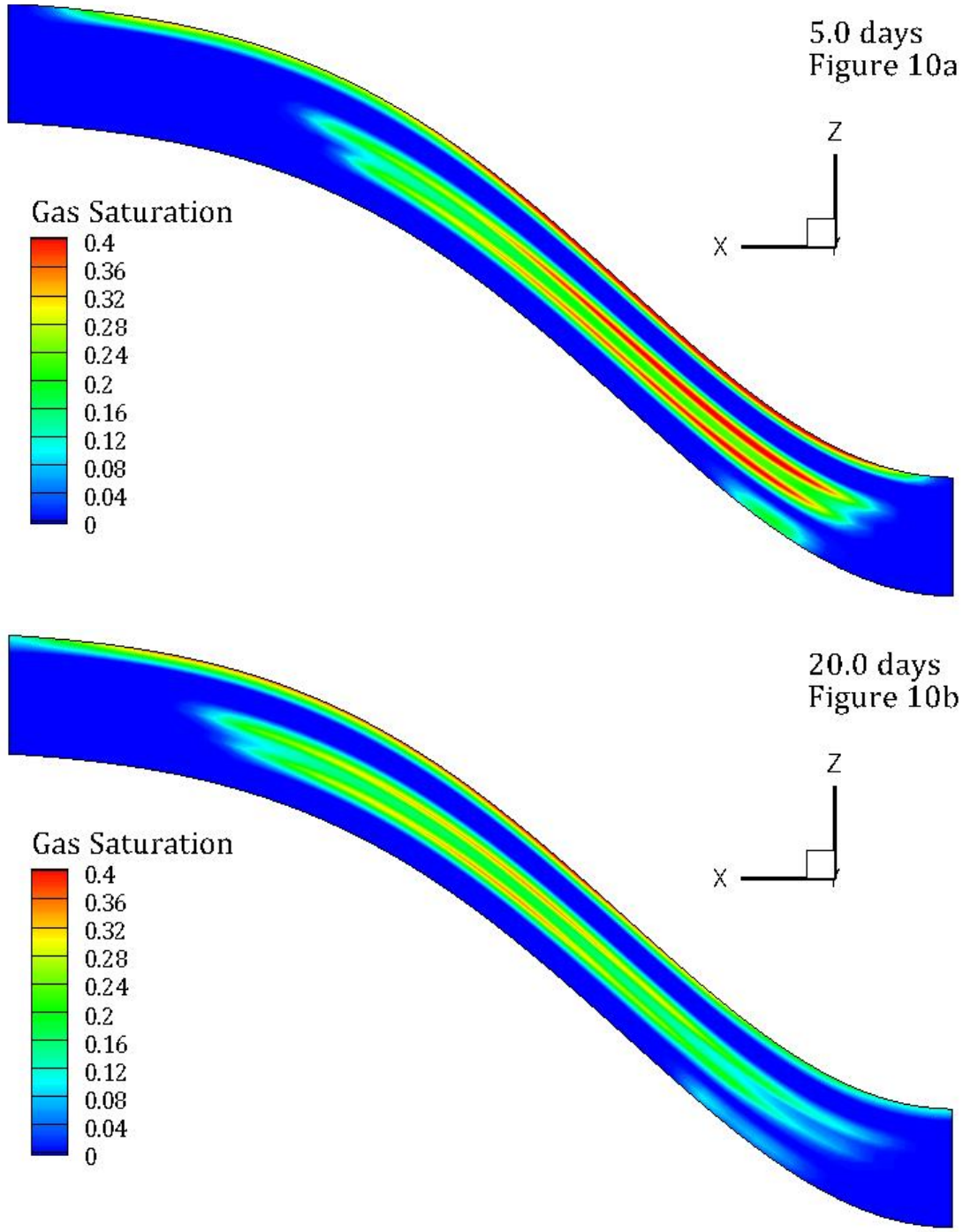

Figures 10a-b. Gas saturation at 5.0 and 20.0 days